JOURNAL OF APPLIED ELECTROCHEMISTRY 21 (1991) 767–773

Computer simulation of high-discharge-rate battery systems

V. J. FAROZIC*, G. A. PRENTICE

Department of Chemical Engineering, The Johns Hopkins University, Baltimore, MD 21218, USA

Received 14 August 1989; revised 21 January 1991

Simulations were carried out for a proposed two-dimensional high-discharge-rate cell under load with an interelectrode gap of the order of 100 μm. A finite difference program was written to solve the set of coupled, partial differential equations governing the behaviour of this system. Cell dimensions, cell loads, and kinetic parameters were varied to study the effects on voltage, current and specific energy. Trends in cell performance are noted, and suggestions are made for development of cells to meet specific design criteria. Modelling difficulties are discussed and suggestions are made for improvement.

Nomenclature

A	surface area of unit cell (cm^2)
A_k	conductivity parameter ($cm^2\,\Omega^{-1}\,mol^{-1}$)
b	Tafel slope (V)
c	concentration ($mol\,cm^{-3}$)
c_0	concentration of bulk electrolyte ($mol\,cm^{-3}$)
D	diffusivity ($cm^2\,s^{-1}$)
D_h	lumped diffusion parameter ($J\,s\,cm^{-2}\,mol^{-1}$)
D_s	lumped diffusion coefficient ($A\,cm^2\,mol^{-1}$)
E	rest potential of electrode (V)
F	Faraday constant (96 500 $C\,mol^{-1}$)
i	current density ($A\,cm^{-2}$)
I	total current for unit cell (A)
i_0	exchange current density ($A\,cm^{-2}$)
N	flux of charged species ($mol\,cm^2\,s^{-1}$)
R	gas constant (8.314 $J\,mol^{-1}\,K^{-1}$)
R_{ext}	resistance external to cell (Ω)
t	time (s)
T	temperature (K)
t_0	transference number
u	mobility ($cm^2\,mol\,J^{-1}\,s^{-1}$)
V	volume of an element in the cell (cm^3)
V_{ext}	voltage external to cell (V)
z	charge on an ion
η_c	concentration overpotential (V)
η_s	surface overpotential (V)
κ	conductivity ($\Omega^{-1}\,cm^{-1}$)
ν	stoichiometric coefficient
Φ	electric potential in solution (V)

1. Introduction

Two-dimensional simulations of a high-discharge-rate battery system are examined in this paper. The proposed configurations are unique in that the interelectrode gap is of the same order of magnitude as the evolving diffusional boundary layer. These cells are being considered because the low internal ohmic resistance associated with a small interelectrode separation makes possible a device that possesses very high specific power. Such batteries could eventually replace bulkier arrays currently used in aerospace and military applications. For example, one cell used for these applications was required to provide 30 A for one minute at 14 V [1]. The advantage of microelectrode construction is a decrease in size and weight from the present standard of 1.22 kg and 1000 cm^3.

The partial differential equations used to model this system can be solved by the finite difference method. This algorithm allows considerable variation in the parameters describing the system, thus enabling a parametric study of the cell performance. The performance variables of interest are voltage and current. Permutations in the major cell parameters (lengths and kinetics) were used to determine the effects on the transient outputs from the cell.

2. Modelled system

Cells having an interelectrode gap of the order of 10 to 100 μm were modelled. Assembly of such a microelectrode array requires an adaptation of the mask and photoresist techniques used in the electronics industry. Hence, the unit cell should be easily fabricated in a repeating fashion on the surface of a substrate. In the light of this, the T-shape shown in Fig. 1 was chosen. This can be thought of as part of a repeating array shown in Fig. 2. Changes in the indicated length scales can be used to alter cell performance to suit a particular purpose. Such a repeating box array is also relatively easy to fabricate.

The zinc/silver oxide couple was chosen for this study because of its high power density and the availability of relevant data [1], (Table 1). Although the

* Present address Rohm and Haas Co., P.O. Box 584, Bristol, PA 19007, USA.

0021-891X/91 $03.00 + .12

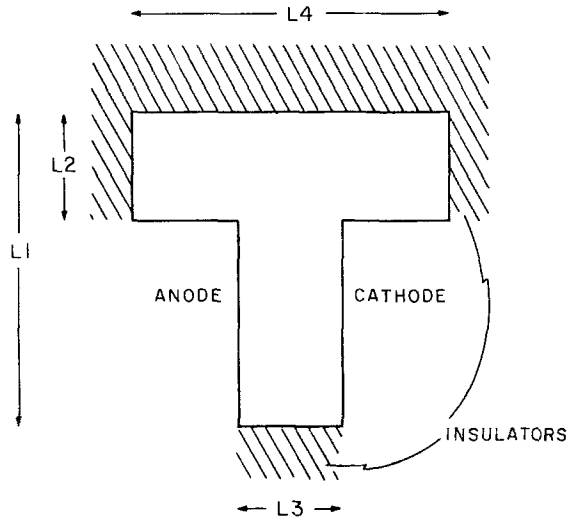

Fig. 1. Unit cell configuration.

detailed electrode reactions are complicated and vary with depth of discharge, for design purposes the overall reaction may be considered to be [1]

$$Zn + AgO = ZnO + Ag \quad (1)$$

On discharge, the model cathode reaction is

$$AgO + H_2O + 2e^- = 2OH^- + Ag \quad (2)$$

The model anode reaction is

$$Zn + 2OH^- = ZnO + H_2O + 2e \quad (3)$$

At equilibrium the stable species is the zincate $Zn(OH)_4^{2-}$, but reaction details are ignored in this study. The electrolyte for the model system is a 7 M aqueous KOH solution.

3. Equations and theory

The basic equations governing the model system were derived from dilute solution theory. Although the electrolyte of interest is relatively concentrated,

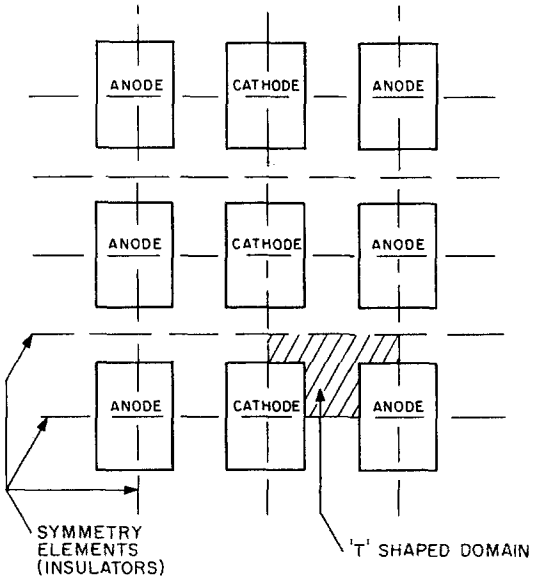

Fig. 2. Array configuration.

Table 1. Properties of the zinc/silver oxide couple used in this work

Characteristic	*Zinc anode*	*Silver oxide cathode*
Tafel slope (V decade^{-1})	0.582	0.200
i_0 (A cm^{-2})	0.235	0.250
Φ_{rest} (V/NHE)	−0.83	0.87
Density (g cm^{-3})	7.14	7.44
Molecular weight (g mol^{-1})	65.37	123.87

approximate results can be obtained through suitable adjustment of the transport coefficients. At the relatively short times of interest, convective flows are not established, and the bulk fluid velocity in a narrow-gap cell is assumed to be zero.

Combination of the expressions for the flux, material balance, and electroneutrality for a binary electrolyte yields [2]

$$D\nabla^2 c = \partial c/\partial t \quad (4)$$

and

$$F\nabla \cdot (c\nabla\Phi) = D_h \partial c/\partial t, \quad (5)$$

where D and D_h are diffusion parameters that follow from the original mass balances,

$$D_h = (D_- - D_+)/(z_+u_+D_- - z_-u_-D_+) \quad (6)$$

and

$$D = (z_+u_+D_- - z_-u_-D_+)/(z_+u_+ - z_-u_-). \quad (7)$$

There are two different boundary types for an electrochemical system: electrodes and insulators. For the insulator, there is no normal flux of charged species. This implies that the normal potential and concentration gradients (the driving forces for ionic transport within the cell) are zero at the insulators, or

$$(\nabla\Phi)_{norm} = 0 \quad (8)$$

and

$$(\nabla c)_{norm} = 0. \quad (9)$$

As an extension of the work of Menon and Landau [3], both concentration and surface overpotentials were incorporated in the model. An expression for the concentration overpotential is necessary because large concentration gradients are built up in high-discharge-rate devices. The expressions used here are

$$\eta_s = b \log (i/i_0) \quad (10)$$

for the surface overpotential and

$$\eta_c = 2RT/F[k_1 \ln (c/c_0) + k_2(1 - c/c_0)] \quad (11)$$

for the concentration overpotential, where

$$k_1 = (3t_0^- + 1)/(t_0^- + 1) \quad (12)$$

and

$$k_2 = t_0^- t_0^+/(t_0^- + 1) \quad (13)$$

Equation 10 is the Tafel equation, where b is the Tafel slope and i_0 is the exchange current density. In

Equation 11, c_0 is the bulk electrolyte concentration, and the t_0's are the transference numbers. Binary electrolyte, linear concentration gradients, and a dilute solution were assumed.

In order to calculate the overpotential losses, it is necessary to determine the current density and concentration at the electrode surface. The expression for current density,

$$i = -A_k c(\nabla\Phi)_{norm} - D_s(\nabla c)_{norm}, \quad (14)$$

allows for the transport of ions to the surface of the electrode by migration or by diffusion. The constants A_k and D_s, again, are derived from the mass balance yielding

$$D_s = z_+ v_+ F(D_- - D_+) \quad (15)$$

and

$$A_k = z_+ v_+ F^2(z_- u_- - z_+ u_+), \quad (16)$$

where the v is the stoichiometric number or the number of ions of a particular charge formed from a binary electrolyte.

The concentration is calculated from that of the previous time step using a differential form of Faraday's law,

$$dc = iA\, dt/nFV \quad (17)$$

The change in concentration implied by this differential is applied over a volume element V adjacent to the electrode surface. The current density at the adjoining electrode surface is used in the calculation of the concentration change.

Once expressions for the surface concentrations and current densities have been calculated, they are put into Equations 10 and 11 to yield the total surface losses. These equations are used to calculate the voltage at the electrode surface,

$$\Phi = E - \eta_c - \eta_s \quad (18)$$

In addition to the previous equations that were inserted into the algorithm, an option to account for the presence of an external finite resistance was included. This constrains the cell according to

$$V_{ext} = IR_{ext} \quad (19)$$

where R_{ext} is the external resistance, I is the integrated sum of the current densities inside the cell, and V_{ext} is the voltage as measured across the terminals of the battery. V_{ext} is calculated by

$$V_{ext} = \Delta E - \eta_c - \eta_s - \Delta\Phi_{ohm} \quad (20)$$

The overpotentials in Equation 20 are for both anode and cathode. ΔE is the difference between the rest potentials of the electrodes, and $\Delta\Phi_{ohm}$ is the ohmic loss in the electrolyte that accompanies the passage of current. Because the electrodes are treated as equipotential surfaces, the sum of the loss components (overpotentials and ohmic drop) must be constant along any current path; therefore, $\Delta\Phi_{ohm}$ was calculated by numerically integrating i/κ along a path near the base of the 'T'. It is assumed that the current paths at this point are straight because this portion of the cell most resembles a parallel plate configuration. The conductivity of the medium κ was assumed from dilute solution theory to be a linear function of the electrolyte concentration or

$$\kappa = A_k c \quad (21)$$

The governing equations were cast into a framework for numerical solution. The method used for these equations was an iterative, implicit, finite difference method. Because the coupled concentration-potential equation is not of known stability, an implicit formulation of the difference equations was chosen for its ability to handle unstable equations. Similar equations [4] have posed special difficulty due to unstable convergence behaviour. Initial attempts to utilize the Alternating-Direction Implict method did not lead to converged solutions. It proved more workable to discretize in both Cartesian directions in a single expression, *cf.* Appendix A. A more detailed description of the algorithm used and the text of the program can be found elsewhere [5].

4. Results and discussion

A two-dimensional simulation was chosen to model these systems because effects acting perpendicular to the battery array (such as gravity induced convection) are considered to be negligible. A basis of 1 cm was chosen for the plane perpendicular to the arrays shown in Figs 1 and 2. A summary of the results presented in the following paragraphs is presented in Table 2.

A worst case in terms of useful battery lifetime is the short-circuit condition. One measure of battery lifetime is the half-life, defined here as the time for the total current to reach one half of its initial value. If the battery is driving a purely resistive load, this corresponds to the voltage half-life as well. Figure 3 shows the discharge curve (normalized current versus half-life) for a cell with a 100 μm interelectrode gap. Initial current is 13 A and the half-life is 7.4 ms. The lengths for this example, defined in Fig. 1, are $L1$ = 0.05 cm, $L2$ = 0.01 cm, $L3$ = 0.01 cm, and $L4$ = 0.04 cm. Figure 4 appears identical to Fig. 3, but is a discharge curve for a proportionally sized cell of similar geo-

Table 2. Results of simulations for the 10 μm-gap cell. Lengths as defined in Fig. 1; L3 equals L2 in all cases

L1 (cm)	L2 (cm)	L4 (cm)	R_{ext} (Ω)	I_{init} (A)	Half life (s)
0.050	0.010	0.040	0.00	12.23	7.4×10^{-3}
0.005	0.001	0.004	0.00	9.30	1.0×10^{-4}
0.050	0.010	0.040	0.07	7.62	3.1×10^{-2}
0.005	0.001	0.004	0.07	6.22	2.2×10^{-4}
0.050	0.010	0.040	0.03	9.38	2.3×10^{-2}
0.005	0.001	0.004	0.03	7.67	1.9×10^{-4}
0.070	0.010	0.030	0.03	8.11	3.7×10^{-3}
0.007	0.001	0.003	0.07	6.12	2.3×10^{-4}
0.009	0.001	0.002	0.07	4.88	2.1×10^{-4}
0.005	0.001	0.004	0.18	4.71	4.5×10^{-4}

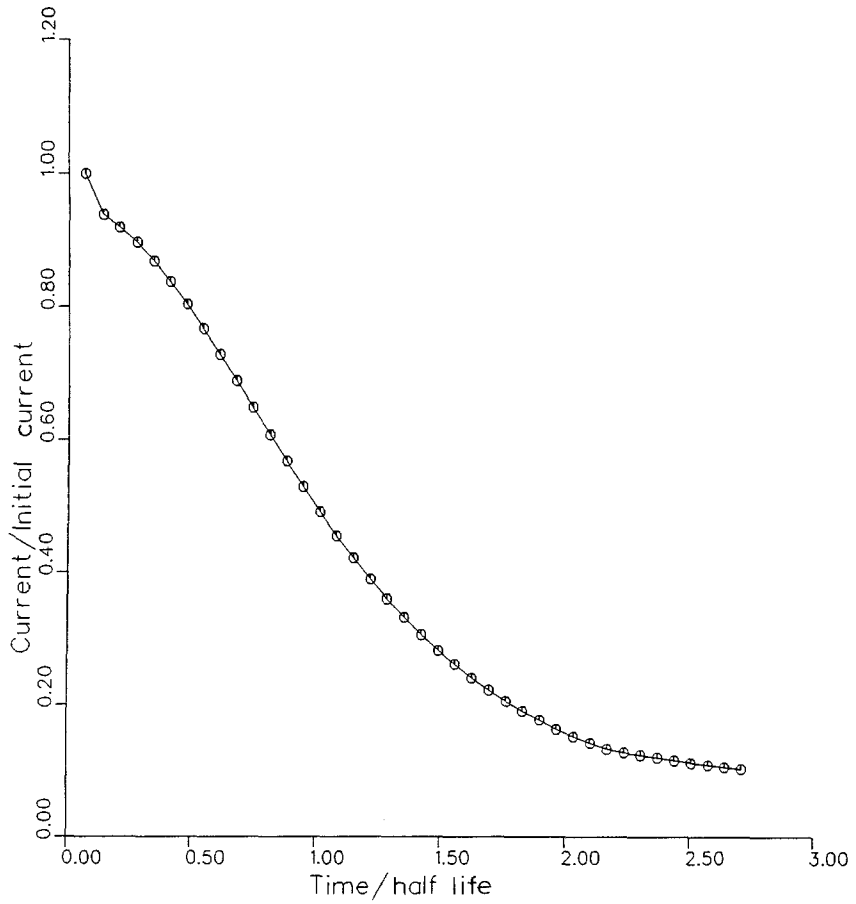

Fig. 3. 100 μm-gap cell short-circuit performance.

metry with an interelectrode gap of 10 μm. The corresponding lengths are $L1 = 0.005$ cm, $L2 = 0.001$ cm, $L3 = 0.001$ cm, and $L4 = 0.004$ cm. The initial current for this cell is 10 A, and its half-life is approximately 0.1 ms. Even though this cell has 1% of the area of the previous cell, its current output is comparable for a short time.

The short-circuit condition gives a measure of how

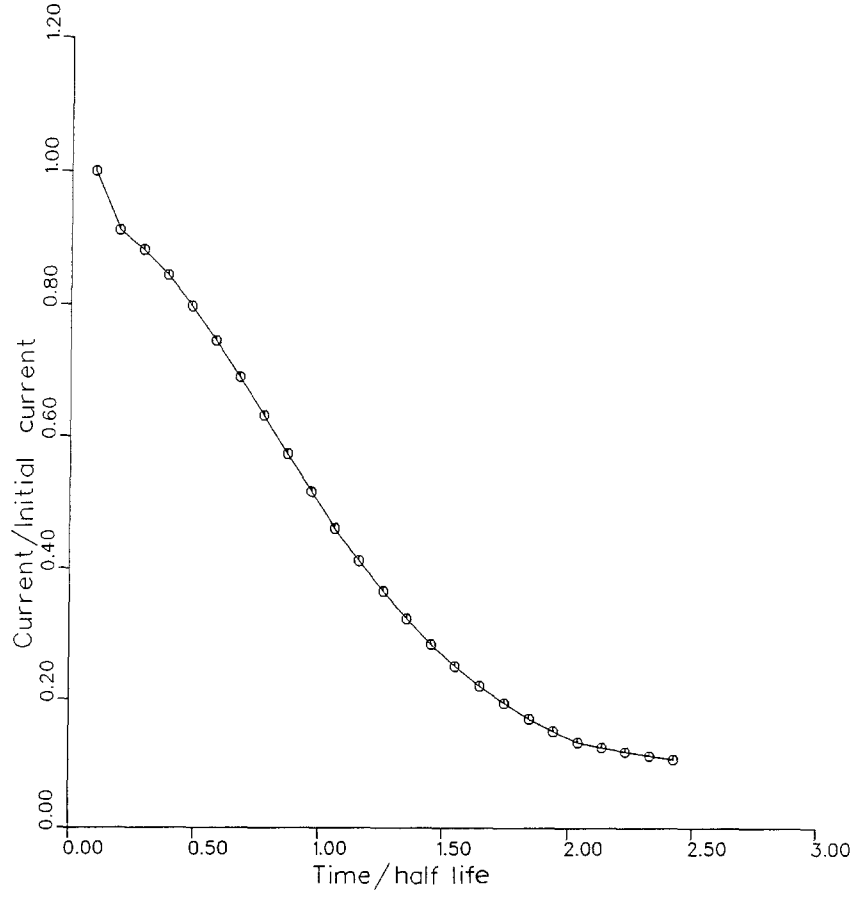

Fig. 4. 10 μm-gap cell short-circuit performance.

quickly the cells deactivate in the worst case. It also illustrates a characteristic of these cells: the initial slopes of the current versus time plots are maintained through the half-life. All runs performed have shown this tendency. The absence of an electrode consumption term in the model implies that the simulated half-life is less accurate for the 10 μm-gap cells because electrode consumption has more effect on interelectrode separation.

The favourable characteristics of microscopic electrodes arise from the fact that the bulk electrolyte resistance is roughly proportional to interelectrode gap. When the gap is small, resistance to rapid discharge resides almost entirely at the electrode/electrolyte interface. The factor that "shuts down" these cells is the diffusion layer formed at the electrode surface. The concentration overpotential associated with these layers can be sizeable. For instance, the overpotential associated with the anode of the 10 μm-gap cell at 2.4 half-lives is 660 mV or 68% of the total losses associated with that electrode. These depletion or enrichment zones are formed more quickly at higher discharge rates; therefore, the areas within the cell which are initially very active tend to "deactivate" first. The depletion of hydroxide in the 10 μm-gap cell near the base of the 'T', effectively shuts down this portion of the cell first. The current in the crossbar of the 'T' becomes proportionately greater as the distribution evolves because the higher bulk resistance due to the longer current paths moderates the electrochemical reaction at these sites. This allows the diffusion of ions to keep a closer pace with the kinetics of reaction and prevents the sharp concentration gradients that shut down the base of the 'T'.

The performance of the 100 μm-gap cell and the 10 μm cell with an external load connected can be directly compared. The smaller cell will obviously not be able to drive loads as well as the larger one. An array of 100 of the smaller cells, however, occupies the same amount of space as one of the larger ones. Figure 5 illustrates two cases: a 100 μm-gap cell with a geometry as in Figure 4 loaded with a 0.07 Ω resistor and 100 10 μm-gap cells with a similar geometry loaded with the same resistor. Superposition of solutions yields the resulting lines. This figure demonstrates the dramatic increase in power delivery that can be attained by using the smaller cells as well as the sharp transients that must be accounted for if such performance and size are desirable.

It is also of interest to observe how load size affects battery performance. There is a notable interaction between the internal chemistry of the cell and the external resistance. Currents for the 10 μm-gap cell of Fig. 3 are presented as a function of time in Fig. 6 for three different loads. The resistance not only changes the available current but also the half-life. The cell loaded by the 0.03 Ω resistor has a half-life of approximately 1.9×10^{-4} s compared with a half-life of 2.2×10^{-4} s for the 0.07 Ω case and 4.5×10^{-4} s for the 0.18 Ω load. The 0.18 Ω case may be considered a practical operating condition because the internal

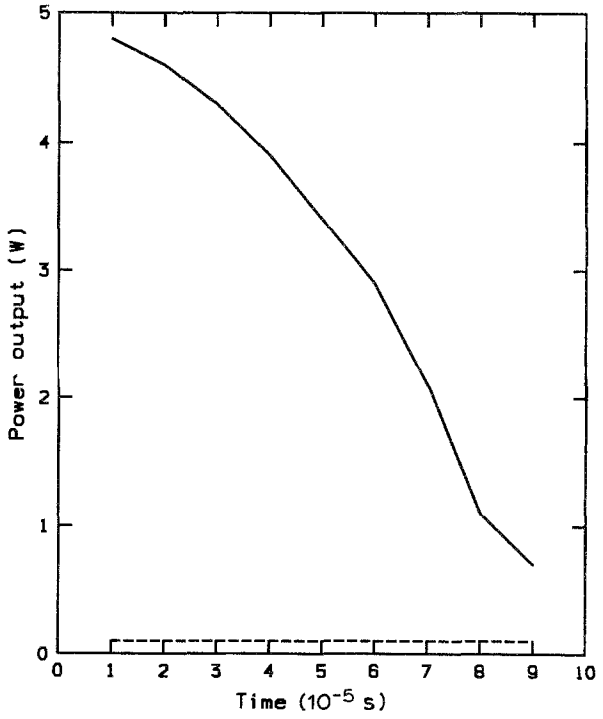

Fig. 5. Power comparison of a 100 μm-gap cell (dashed line) with an array of 100 10 μm-gap cells (solid line) driving a 0.1 Ω resistor.

resistance of the cell is approximately equal to the external resistance. This condition is necessary for maximum power delivery through the load [6]. Such variations in initial output and half-life may be of importance depending upon the system to be driven.

Because the main region of the cell that limits the half-life is the upright region of the 'T', it is important to consider the effect of changing the length scales on the half-life of the cell. Changing the ratio of upright electrode area to crossbar electrode area has some

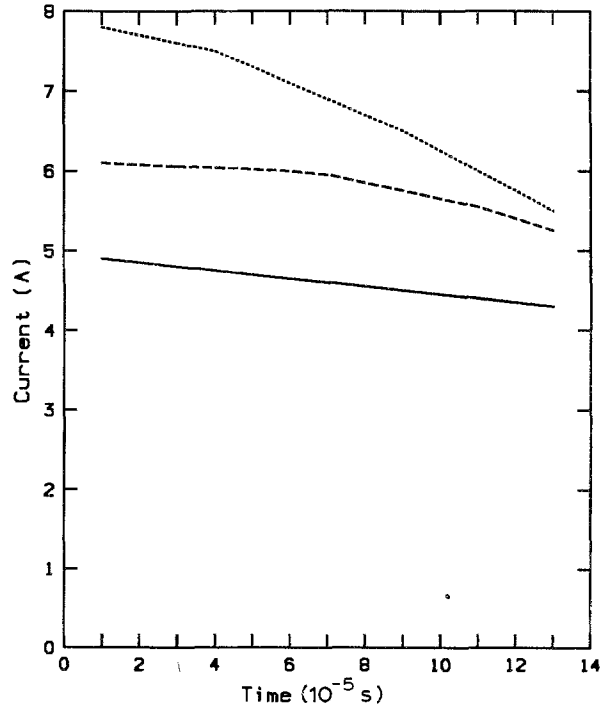

Fig. 6. Effect of load on a 10 μm-gap cell: 0.18 Ω (solid line), 0.07 Ω (dashed line), and 0.03 Ω (dotted line).

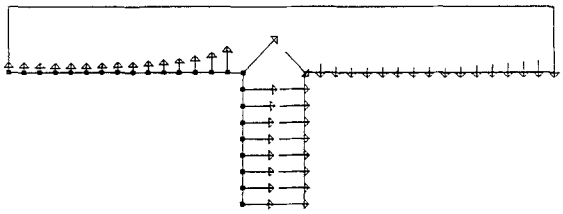

Fig. 7. Initial current distribution for a 10 μm-gap cell. Outward pointing vectors are proportional to the anodic current density; inward pointing vectors indicate cathodic current density.

effect on initial current output and half-life. The area ratio has a very small effect on the half-life of the 10 μm-gap cell loaded with a 0.07 Ω resistor, but there is a fairly demonstrable decrease of the current output if the ratio of the upright area to the crossbar area is less than unity. This occurs because an increase in crossbar area causes an increased ohmic drop between the ends of the crossbar. In other words, the tips of the crossbar are less active than the case shown in Fig. 7.

Surface overpotential is another parameter studied. Figure 8 shows the performance of the 10 μm-gap cell through a 0.03 Ω resistor with the anodic Tafel slope b reduced to one-fifth of its base-case value. This reduction in Tafel slope corresponds to an approximately 80% reduction in the kinetic resistance at the anode. The results illustrate that the discharge rate of the cell with the shallower Tafel slope is 20% higher initially but has a 20% smaller half-life due to the buildup of strong concentration gradients.

Energy efficiency has a direct impact on size and weight. Specific energy would be expected to increase as electrolyte mass decreases because the electrolyte mass contributes to internal ohmic resistance as well as to weight; however, inefficiencies owing to high overpotentials (at a specified load) can overshadow the effects of reduced electrolyte volume. The theoretical specific energy calculated on an electrolyte-free basis for the zinc/silver oxide couple is 450 W h kg^{-1}. Integration of the output power over the time required to consume all of the electrode material gave a rough estimate of the system's specific energy. On this basis the 100 μm-gap cell had a specific energy of 100 W h kg^{-1} or 20% of theoretical. For the narrower cell 50 W h kg^{-1} was estimated (10% of the theoretical value). These values are low because rapidly developing concentration effects persist throughout the integration, a period of many half-lives. The required support system was not taken into account. Other factors such as thermal management and electrode passivation would need to be considered in a realistic design.

Several nonidealities were incorporated in approximate fashion and others were ignored. The equations derived for ionic transport apply strictly to infinitely dilute solutions. At 7 M (the bulk electrolyte concentration for all runs), this assumption is invalid. However, this deviation may be taken into account in the transport constants in the equations. Such compensation was used by Menon and Landau with good results [3].

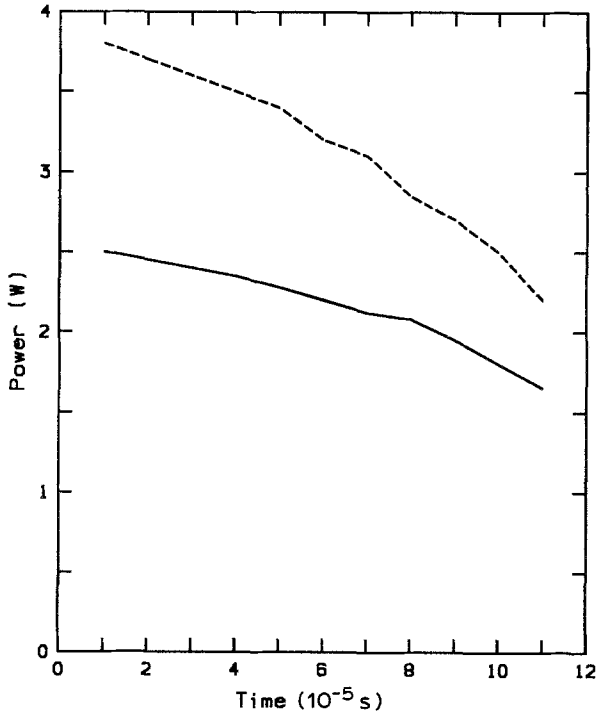

Fig. 8. Effect of anodic Tafel slope on 10 μm-gap cell performance. Solid line is the base case and dashed line represents Tafel slope reduced to one-fifth of the base case value.

Zinc passivates under many conditions in alkaline electrolyte. Although the nonidealities of the zinc electrode have been examined in numerous studies [1], no galvanostatic experiments have been done on zinc with the high current densities (100 to 1000 A cm^{-2}) present in the model system.

Some other considerations that were not incorporated in the model are the effects of heat and moving boundaries. In a system with such high-discharge-rates the heating of the cell can be estimated by calculating the ohmic and overpotential drop within the cell. An approximate calculation indicates that the heating is on the order of 2 W for both the 10 μm-gap cells and the 100 μm-gap cells. This corresponds to enough heating to raise the temperature of the solution in the smaller cell approximately 10° C assuming the interior of the cell to be adiabatic during such a quick heat generation. A rigorous calculation would require adjustment of some of the cell parameters such as the Tafel slope and the transport constants to accommodate this temperature increase. However, this should be interpreted as a second order effect given the other approximations introduced in the smaller cell. The larger cell has a greater heat storage capacity so its temperature increase is on the order of 1° C. Although the consumption of electrode material poses a more serious challenge, it is possible to perform a series of simulations with consistently smaller electrodes corresponding to the amount of electrode material lost to reaction. Preliminary calculations indicate that the cell half-life (defined above) for the 10 μm-gap cell differs if an allowance is made for a decrease in kinetic rates beyond model calculations due to an increase in the electrode gap. This effect

will probably cause significant deviation from the modelled results as the half-life is approached.

5. Numerical analysis

There are several types of adjustable factors available for manipulation once the physical system is defined. The time and distance step sizes are major points that contribute to errors. It is known [7] that making these parameters as small as possible without using excessive computing time can minimize potentially serious difficulties. Another adjustable group of parameters contains the relaxation factors used to speed convergence. These do not influence the results obtained from simulations [4]. A final type of adjustable parameter is the error criterion used to specify the degree of convergence of the problem. All of these have been set to levels between 1×10^{-6} and 5×10^{-5} throughout the program. In all cases, tighter convergence was not found to alter the solution appreciably. Looser convergence, although possible, leads to greater errors carried from time step to time step, an extremely undesirable situation for this type of simulation.

Throughout this study, there was a consistent discrepancy in the integrated current between the anode and the cathode. The anode current starts at a relatively high value and drops steadily in time. The cathode starts slightly lower (*ca.* 15%), peaks to a maximum value, and then falls. In all cases, the cathode current remained above the anode current by roughly an ampere. This inconsistency can be lessened by refining the time step for a 100 μm-gap cell from 0.005 s to 0.0001 s. This improvement reduces the current discrepancy to less than 0.5 A at all times, but takes fifty times as long to run a simulation. Changing the distance discretizations and the convergence factors brought about no appreciable improvements of this problem. A more detailed numerical analysis of this problem can be found elsewhere [5].

6. Conclusions

Simulations of high-discharge-rate devices are useful in guiding the design of a battery for a specific application. The battery system performance can be tailored to a specific application by changing the interelectrode gap. The sharp initial current spike or transient seen in the 10 μm-gap case may be overcome by a combination of improved chemistry and wider gaps. On the other hand, if a current spike with the steepest possible slope is desired, one should make the gap as narrow as is practical.

A more general suggestion for the geometry of the array is to make the upright-to-crossbar area ratio in a 'T' cell unity. This will yield a high current capacity and a favourable half-life. Such a geometry corresponds to square electrodes in Fig. 2. The importance of considering the load to be driven is also stressed. Thus, the entire system of battery and load should be considered as part of the design process because the brevity of the half-life and severity of the transients are strongly influenced by the load.

Acknowledgment

This work was partially supported by a subcontract from the U.S. Office of Naval Research.

References

[1] 'Zinc-Silver Oxide Batteries', (edited by A. Fleischer and J. J. Lander), John Wiley, New York (1971).
[2] G. A. Prentice, 'Electrochemical Engineering Principles', Prentice Hall, Englewood Cliffs, NJ (1991) pp. 151–6.
[3] M. Menon and U. Landau, 'Modelling of Electrochemical Cells Including Diffusion, Migration and Unsteady State Effects', Toronto Symposium of The Electrochemical Society on Engineering of Electrolytic Processes (1987).
[4] D. W. Peaceman, 'Fundaments of Numerical Reservoir Simulation', Elsevier, New York (1977).
[5] V. J. Farozic, 'Simulation of High-discharge-rate Battery Systems', Master's Thesis, The Johns Hopkins University, Baltimore, MD (1989).
[6] E. B. Wilson, 'An Introduction to Scientific Research', McGraw-Hill, New York (1952).
[7] M. E. Davis, 'Numerical Methods and Modeling for Chemical Engineers', John Wiley, New York (1984).

Appendix

The discrete form of the coupled potential-concentration Equation 5 is given by

$$\Phi_{i,j}^{t+1} = [A + B + C]/[-2c_{i,j}^{t}(1/\mathrm{d}x^2 + 1/\mathrm{d}y^2)] \tag{22}$$

where

$$A = D_{\mathrm{h}}(c_{i,j}^{t+1} - c_{i,j}^{t})/\mathrm{d}t \tag{23}$$

$$B = -1/\mathrm{d}x[c_{i,j}^{t}(\Phi_{i+1,j}^{t+1} - \Phi_{i-1,j}^{t+1}) + c_{i+1/2,j}^{t} - \Phi_{i-1/2,j}^{t+1}) + c_{i-1/2,j}^{t}(\Phi_{i-1/2,j}^{t+1} - \Phi_{i+1/2,j}^{t+1})] \tag{24}$$

and

$$C = -1/\mathrm{d}y[c_{i,j}^{t}(\Phi_{i,j+1}^{t+1} - \Phi_{i,j-1}^{t+1}) + c_{i,j+1/2}^{t}(\Phi_{i,j+1/2}^{t+1} - \Phi_{i,j-1/2}^{t+1}) + c_{i,j-1/2}^{t}(\Phi_{i,j-1/2}^{t+1} - \Phi_{i,j+1/2}^{t+1})]. \tag{25}$$

The half step terms are calculated by a three point estimate that is valid for equal node spacing. In general terms this is

$$X_{i+1/2} = 0.375X_{i+1} + 0.75X_{i} - 0.125X_{i-1}. \tag{26}$$

The subscripts $i + 1$, $i - 1$, $j + 1$, and $j - 1$ refer to the nodes adjacent to the general node (i, j) in the mesh in the respective rectangular Cartesian axes. Values halfway between the (i, j) node and its nearest neighbor on a given side are designated by a 1/2. The superscripts t and $t + 1$ designate the value at the present time and time plus one time step respectively. $\mathrm{d}x$, $\mathrm{d}y$, and $\mathrm{d}t$ are the step sizes in the i, j, and t directions. All other terms are defined elsewhere in the text.